Letter

Self-adaptive catch-up injection of positrons in plasma wakefield acceleration

L. Q. Han,[1,2,§] Y. R. Shou,[3,§] H. Wen,[1] J. Cai,[2] X. Y. Zhao,[1] L. Xu,[1] X. D. Liu,[1] J. X. Wang,[1] B. F. Shen,[4] Z. Gong,[5,*] J. Q. Yu,[1,†] and X. Q. Yan[2,6,7,‡]

[1]*Hunan Provincial Key Laboratory of High-Energy Scale Physics and Applications, School of Physics and Electronics, Hunan University, Changsha, 410082, China*

[2]*State Key Laboratory of Nuclear Physics and Technology and Key Laboratory of HEDP of the Ministry of Education, CAPT, Peking University, Beijing, 100871, China*

[3]*Center for Relativistic Laser Science, Institute for Basic Science, Gwangju, 61005, Republic of Korea*

[4]*Shanghai Normal University, Shanghai, 200234, China*

[5]*CAS Key Laboratory of Theoretical Physics, Institute of Theoretical Physics, Chinese Academy of Sciences, Beijing 100190, China*

[6]*Collaborative Innovation Center of Extreme Optics, Shanxi University, Taiyuan, Shanxi, 030006, China*

[7]*Guangdong Laser Plasma Institute, Guangzhou, 510540, China*

(Received 15 January 2025; accepted 2 June 2026; published 17 July 2026)

The injection of positrons in a plasma wakefield has long been challenging due to the demand for an appropriate field structure. Here, we propose a novel approach whereby a positron source is positioned at the front of a hollow, positively charged driver. This configuration allows the plasma wakefield to continuously catch up with the positrons, enabling self-adaptive capture into the accelerating and focusing phase. Our analytical model demonstrates that positrons with varying angles, energies, and initial positions can be effectively injected into similar phases for further acceleration. In addition, introducing a transversely asymmetric driver can substantially enhance the energy gain without affecting the injection. Three-dimensional quasistatic PIC simulations show that injected positrons with a charge of 12 pC can be accelerated to energies exceeding 14 GeV using a 10 GeV hollow positron driver, corresponding to an acceleration gradient of 16 GV/m. These results provide a proof-of-principle demonstration for a new positron injection and acceleration scheme in plasma wakefields.

DOI: 10.1103/n95z-ty9l

Plasma wakefield acceleration, driven by high-power lasers (LWFA) [1] or high-charge particle beams (PWFA) [2], can achieve an acceleration gradient three orders of magnitude higher than that in conventional radio frequency (rf) accelerators [3–5]. The last two decades have witnessed significant progress in both the theoretical and experimental aspects of PWFA for electrons [6–13]. However, the electron acceleration schemes are not directly applicable for accelerating positrons. With a negatively charged driver, the only region where the positrons get simultaneously accelerated and focused is the central axis where the plasma electrons cross [14]. The common method to expand the focusing area of positrons is either using a specially structured driver or plasma to form an electron filament along the central axis, or using a hollow plasma channel to eliminate the defocusing field of ions [15–21]. On the other hand, although a positively charged beam has the potential to accelerate and focus self-loaded positrons effectively [22,23], the focusing field exhibits radial nonlinearity and undergoes variations along the beam axis, which results in an increase in the emittance of the witness beam [24].

Beyond generating a favorable field structure, a central challenge is how low-energy positrons from an external source in experiment [25–28], characterized by a broad energy spread and a disordered phase-space distribution, can be controllably and precisely injected into the phase region that simultaneously provides focusing and acceleration [29,30]. In many previous simulation studies, a preaccelerated positron beam is directly assumed to be placed in the appropriate accelerating phase. While such a setup is useful for studying the subsequent acceleration process, how low-energy positrons overcome the space-charge forces and the wakefields to enter the focusing and accelerating region [31], and how to manipulate the phase

*Contact author: zgong92@itp.ac.cn
†Contact author: jinqing.yu@hnu.edu.cn
‡Contact author: x.yan@pku.edu.cn
§These authors contributed equally to this work.

Published by the American Physical Society under the terms of the Creative Commons Attribution 4.0 International license. Further distribution of this work must maintain attribution to the author(s) and the published article's title, journal citation, and DOI.

with the required spatiotemporal synchronization precision on the micrometer scale [32], remain largely unclear. The method of preaccelerating a positron beam with initial energy and subsequently cascading it into further stages also presents significant challenges in coupling efficiency [11,33,34], requiring a good beam-to-plasma matching [35]. Thus, there is a demand for a scheme that can efficiently and controllably inject low-energy positron sources into the appropriate focusing and accelerating phase for further acceleration.

In this Letter, we report a novel injection scheme using a hollow, positively charged (positron or proton) beam. In this scheme, as long as the external positron source is positioned ahead of the driver, the wakefield can continuously catch up with and self-adaptively capture the positrons into the suitable accelerating and focusing phase for further acceleration. The positively charged driver attracts the background plasma electrons, resulting in the formation of a high-density annular structure around its central axis and an electron filament along the axis, as shown in Fig. 1. Positrons with energies ranging from several MeVs to tens of MeV can be captured by the wakefield. In addition, a transversely asymmetric driver can significantly increase the energy gain.

Hollow positron beams could be formed similarly to hollow electron beams in simulations by employing Laguerre-Gaussian laser pulses [37–39], and extended to higher energies [40]. The density distribution of the driver is [15]

$$n_p = n_0 \exp\left[-\frac{(r-r_0)^2}{2\sigma_r^2} - \frac{(\xi-\xi_0)^2}{2\sigma_z^2}\right], \tag{1}$$

where $\xi = z - ct$ is the co-moving coordinate, with $\xi = 0$ denoting the origin of this coordinate system. The peak number density of the driver is $n_0 = 1 \times 10^{17}$ cm^{-3}, equal to the preformed hydrogen plasma density. Here, r_0 and ξ_0 are the transverse and longitudinal locations of the peak driver density, respectively. We used 3D PIC code WarpX [41] to study the unloaded wakefield structure. The simulation box $x \times y \times z = 90 \times 90 \times 200$ μm is divided into $256 \times 256 \times 512$ cells, with a moving window in the z direction. The charge of the hollow positron beam is 4.2 nC, with $r_0 = 30$ μm, $\xi_0 = 0$, $\sigma_r = 15$ μm, $\sigma_z = 15$ μm, and an energy of 10 GeV. A high-density electron filament with a density of $\sim 1.2 n_0$ is formed on the axis as shown in Figs. 1(a) and 1(b). The length of the effective acceleration region is ∼54 μm, while the length of focusing region is ∼67 μm. The overlap is between $\xi = -65$ μm and $\xi = -19$ μm, as shown in Figs. 1(c)–1(e), where positrons need to be injected.

We have developed a two-dimensional theoretical model of the injection process based on quasilinear approximations to analyze the injection process. Assuming that the positrons lie in the plane $y = 0$, with $p_y = 0$ and $|x| = r$.

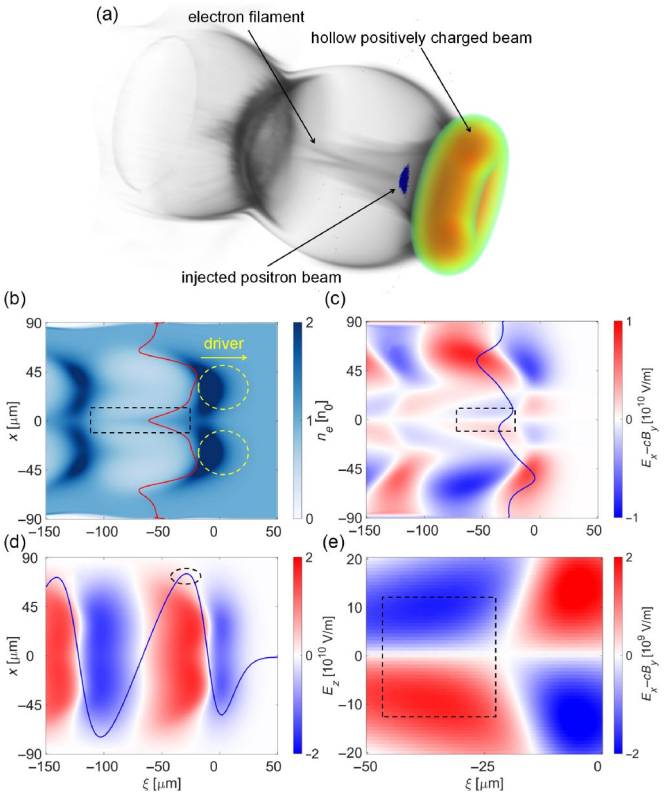


FIG. 1. (a) Schematics of positron acceleration in a plasma wakefield driven by a hollow, positively charged beam in a 3D PIC simulation. The injected positrons (blue dots) are focused by the electron filament on the axis [36]. (b) Density distribution of the plasma electrons, with a clear high-density region along the central axis, where the driver is located at the position outlined by the yellow dashed box. (c) Transverse field and (e) enlarged view, a focusing field on positrons formed by plasma filament along the central axis, the effective focusing region is shaped like an isosceles triangle, a base width of ∼52 μm, a height of ∼67 μm, and a bottom width of ∼126 μm. The dashed rectangles highlight the accelerating and focusing region. (d) Longitudinal field, the effective acceleration length for positrons is ∼54 μm.

The peak drive density is equal to n_0, so that linear perturbation theory can be applied [15,42,43]. The cylindrically symmetric transverse and longitudinal wakefield can be expressed as $E_z(r,\xi) = Z'(\xi)R(r)$ and $W_\perp(r,\xi) = -Z(\xi)R'(r)$, where

$$Z'(\xi) = 4\pi \int_{-\infty}^{\xi} e n_\parallel(\xi') \cos k_p(\xi - \xi') d\xi', \tag{2}$$

$$R(r) = k_p^2 \int_0^{\infty} n_\perp(r') r' K_0(k_p|r - r'|) dr', \tag{3}$$

where $n_\parallel(\xi) = n_0 \exp(-(\xi-\xi_0)^2/2\sigma_z^2)$, $n_\perp(r) = \exp(-(r-r_0)^2/2\sigma_r^2)$, K_0 is the modified Bessel function of zero order, $k_p^{-1} = c/w_p = 16.8$ μm. Therefore, the numerical solutions of E_z and W_r at different ξ and r can be obtained.

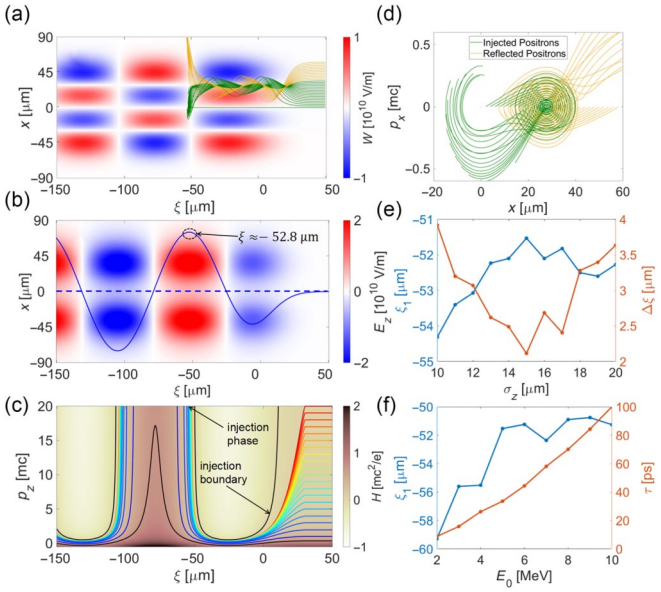


FIG. 2. The theoretical injection results. (a) The linear numerical integration solution of the transverse wakefield and the trajectory of witness positrons, the green (yellow) line represents the trajectory of injected (reflected) positrons. (b) The numerical integration solution of the longitudinal wakefield and 1D slice along the axis, with peak accelerating gradient located at $\xi = -52.8$ μm. (c) The colored background contour lines with brown color map rendering the Hamiltonian value $H(\xi, p_z)$, and the black contour lines revealing the longitudinal injection boundaries. (d) The trajectory of witness positrons in transverse phase space. (e) Injection phase ξ_1 and phase deviation between peak acceleration gradient and the injection phase $\Delta\xi$ of drivers with different longitudinal length σ_z. (f) Injection phase ξ_1 and injection time τ of witness positrons with initial energy E_0.

The initial energy of the witness positrons is 5 MeV, and the initial impact parameters x_0 are distributed between 0 and 60 μm with $\xi_0 = 45$ μm, with the motion trajectory calculated based on the Lorentz equation as shown in Fig. 2(a).

When witness positrons enter the annular focusing field, they oscillate around the central position of the driver ($x = \pm r_0$) as shown in Fig. 2(a), so the longitudinal field can be approximated by the field at $x = \pm r_0$. Therefore, the longitudinal motion can be described using Hamiltonian theory [44–48]

$$H(\xi, p_z) = \sqrt{1 + p_z^2} - p_z + \Phi(\xi), \tag{4}$$

where H is the Hamiltonian of positrons, Φ is the electric potential of the wakefield, normalized to mc^2/e. The numerical solution of the longitudinal electric field $E_z(\xi)$ and 1D slice at $x = 0$ is shown in Fig. 2(b). Then the electric potential Φ is calculated via $\Phi(\xi) = \Phi(-\infty) - \int_{-\infty}^{\xi} E(\xi)d\xi$, and the distribution of Hamiltonian can be calculated based on Eq. (4) as shown in Fig. 2(c). In the quasistatic regime, the Hamiltonian is not an explicit function of time, i.e., $\partial H/\partial t = dH/dt = 0$, thus the colored contour lines describe the trajectories of witness positrons with different initial longitudinal momentum p_{z0} at $\xi_0 = 50$ μm in the longitudinal phase space. All positrons with $p_{z0} > 0.36$ can be injected, and when $p_{z0} > 10$, the positrons are mostly injected into the same phase, demonstrating the adaptability of the scheme. The longitudinal boundaries of positron injection are indicated by the two black contour lines because the focusing field is located at $\xi < -50$ μm.

On the other hand, positrons with different initial impact parameters x_0 exhibit varying oscillation phases, and the transverse momentum at the end of the first half period determines whether injected or reflected as illustrated in Fig. 2(a). Under the current parameters, we calculate that the transverse boundary is highly symmetric with respect to the center of the driver, i.e., positrons with $|x_0|$ within $0 - r_0$ are successfully injected, whereas those beyond r_0 are expelled. The trajectories of the positrons in the transverse phase space are presented in Fig. 2(d). Positrons initially rotating counterclockwise are reflected, while those rotating clockwise are successfully injected. The weak dependence of the injection phase on the driver parameter σ_z can be observed in Fig. 2(e), even though σ_r has a significant impact on E_z thus changing the longitudinal boundary. Nevertheless, the phase difference $\Delta\xi$ between the injection phase ξ_1 [defined as the mean phase at which positrons first reach the axis $(x = 0)$ after entering the accelerating field without considering phase shifts during the subsequent acceleration process] and the peak accelerating gradient phase reaches the minimum when σ_z is the same as σ_r, i.e., 15 μm.

Figure 2(f) plots the injection phases ξ_1 and injection time τ of positrons with different initial energies calculated by the Lorentz equations. The injection phases are the same as those indicated by the contour lines of the Hamiltonian distribution, showing the validity and self-consistency of the theory. Positrons with higher energy require more stringent conditions for the initial emittance due to the larger τ. Overall, the theoretical model indicates that particles without emittance and self-space-charge effects within the injection boundaries can be self-adaptively injected into the accelerating and focusing phase with a 100% efficiency.

We conducted full 3D PIC simulations to verify the injection of a positron source from the BH process with energies of several MeV, a broad energy spread, and finite divergence [25]. The witness positrons are assumed to enter the plasma after transport, and the initial spectral-angular distribution is shown in Fig. 3(c). To focus on the injection and acceleration process itself, we simplify the positron source to a cylindrical uniform distribution, with the radius 30 μm and the length 40 μm, a density of $0.04n_0$, initially located at the front of the driver. The injection trajectories are illustrated in Fig. 3(a), which are similar to the linear

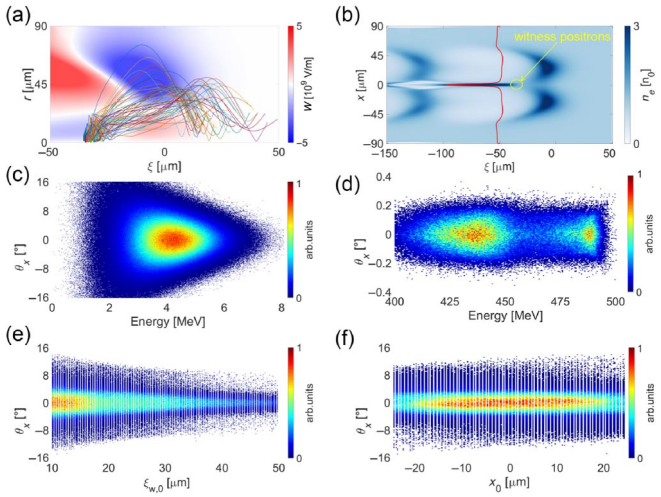


FIG. 3. (a) 3D PIC simulation results of the trajectory of witness positrons in the transverse field. (b) Plasma electron density distribution after injection. The yellow circled area indicates the injected positrons, and the beam-loading effect further enhances the plasma electron density nearby the central axis. (c) The spectral-angular distribution before and (d) after injection. (e) The distribution of the initial longitudinal position and (f) transverse position, and the initial angle of the injected positrons.

case although stable and orderly oscillations are not observed in the nonlinear case with initial emittance. It can be observed that witness positrons with different angles, energies, and initial positions can all be injected into nearly the same phase, indicating the self-adaptive capture behavior of the scheme. When a portion of the positrons are injected, a strong beam-loading effect [49–51] is generated as shown in Fig. 3(b), which prevents further injection. After propagating a certain distance, the relative positions of the injected positrons shift; the beam-loading effect weakens, and a second injection begins, resulting in two peaks in the energy spectrum of the positrons as shown in Fig. 3(d).

The injected charge and efficiency depend on the energy, angular and spatial distribution of the source. The initial longitudinal position $\xi_{w,0}$ of the positron determines the range of angles that can be injected. Most positrons within $\pm 8°$ can be injected, and the injection angular boundary narrows as $\xi_{w,0}$ increases, with the transverse position x_0 has limit effect providing that $x_0 < r_0$, as shown in Figs. 3(e) and 3(f). In total, positrons with small $\xi_{w,0}$ and E_0 are quickly captured, and for larger $\xi_{w,0}$, positrons with larger θ_0 and E_0 will leave the accelerating region before being captured. An injection charge of 12 pC can be obtained with an injection efficiency of approximately 50% for the initial positron background adopted here. The injection efficiency is largely determined by the number of witness positrons that lie within the injection boundary when the driver catches up with the positron source.

It is necessary to consider the changes in the wakefield structure caused by the evolution of the hollow driver during the long acceleration distance. Drive particles with $\psi > 0$ will continuously move toward the axis at the tail, forming a secondary wakefield that attracts more particles [52], where $\psi = \Phi - cA_z$ is the pseudopotential of the wakefield satisfying the Poisson-like equation $\nabla_\perp^2 \psi = -\frac{1}{\epsilon_0}(\rho - J_z/c)$ [7]. Eventually, the hollow structure is lost and so is the accelerating and focusing region. A larger r_0 can restrain the evolution by extending the time needed for the drive particles to reach the axis, as well as reducing positrons with $\psi > 0$. However, if r_0 is so large that no more drive particles can be attracted to the axis by the secondary wakefield, the intensity of the wakefield is not sufficient to inject positrons, and the acceleration gradient is very low. We found that a transversely asymmetric driver can prevent drive particles from moving toward the axis by altering the initial distribution of ψ, while ensuring that injection is unaffected, resulting in a stable structure featuring four high-density regions and a nearly 100-fold extension of the acceleration duration. A detailed discussion will be provided in Supplemental Material [53].

After the positron injection is completed and the beam is accelerated to ~400 MeV in the simulation with WarpX, the full information of the particles and fields is placed into the quasistatic PIC code HiPACE++ [54] to further simulate the acceleration process. In the case of an asymmetric driver, the positrons can be accelerated to more than 14 GeV in 0.9 m, achieving an acceleration gradient of 16 GV/m. Figure 4(a) presents the positrons spatial distribution at the final moment of the simulation, showing that the energy of the beam gradually decreases

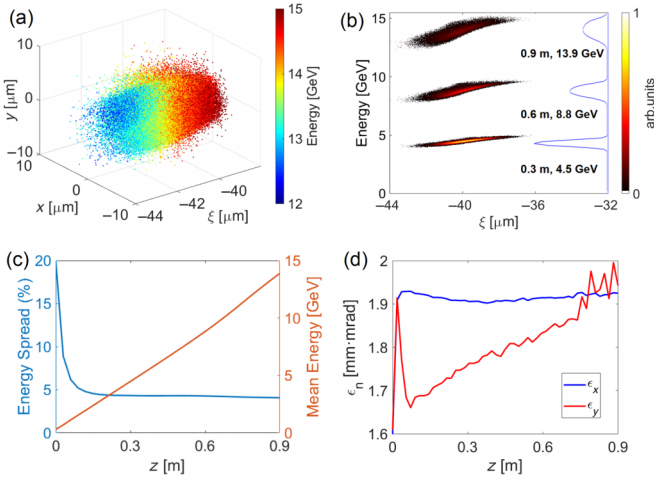


FIG. 4. (a) The spatial position and energy distribution of witness positrons at 3 ns. (b) The longitudinal phase-space distribution (the color map) and energy spectra of witness positrons (blue curves) during acceleration. (c) Evolution of the energy and energy spread and (d) normalized emittance of the witness positron beam vs distance.

from front to back due to the phase slip. The energy spread is approximately 20% shortly after injection and continuously decreases to 4.3% during the acceleration process, while the average energy exceeds 14 GeV, as shown in Figs. 4(b) and 4(c). Due to the evolution of the asymmetric driver, the total emittance along different directions, i.e., ϵ_x and ϵ_y are not identical as shown in Fig. 4(d), but eventually stabilize to the same value of about 1.9 mm mrad. The energy transfer efficiency of the acceleration (defined as the ratio of the energy gained by the witness beam to the energy transferred to the wakefield by the driver [18]) is 1.3%.

Longer acceleration distance can be achieved by using drive particles with higher energy due to greater mass. The energy of a proton beam can be accelerated to a very high level, and the radiation it produces is much less than that of leptons due to its high mass. Thus it is more suitable as a high-energy wakefield acceleration driver [10,11,55]. The injection and acceleration mechanism proposed is determined mainly by the field structure of a positively charged hollow driver. To illustrate the possible extension of the mechanism to higher-energy positively charged driver, we replace the driver with a proton beam while ensuring that both the density distribution and size remain consistent with those of the positron beam, and set the energy to 500 GeV. Positrons can obtain an energy gain of over 214 GeV without affecting the injection process (see Supplemental Material [53]). Therefore, for future high-energy applications, proton drivers are likely to be more suitable, although no practical scheme is currently available for generating such short and hollow proton beams. For this reason, the main text uses hollow positron drivers as a tractable platform to demonstrate the proposed injection mechanism. Possible approaches that mimic a hollow proton-driven wakefield, such as overlapping coaxial proton and electron beams, may provide an alternative route in the future [20].

In conclusion, we have demonstrated a novel scheme of self-adaptive catch-up injection and acceleration of positrons in plasma wakefield acceleration driven by a hollow, positively charged beam. Witness positrons with different initial conditions can all be injected into nearly the same phase and further accelerated. These results provide a proof-of-principle demonstration of a new positron injection and acceleration route in positively charged plasma wakefields and may inform future proton-driven positron acceleration schemes.

This work was supported by the Strategic Priority Research Program of the Chinese Academy of Sciences (Grants No. XDB1550102 and No. XDB1550000), the National Natural Science Foundation of China (Grants No. 12175058 and No. 12575251), and the National Science Fund of Hunan Province for Distinguished Young Scholars No. 2024JJ2009. Z. G. acknowledges the support from the CAS Project for Young Scientists in Basic Research (Grant No. YSBR-141) and the HPC Cluster of ITP-CAS for providing computational resources. J. Q. Y. would like to thank the support from the junior visiting professor program of Peng Huanwu Innovation Research Center for Theoretical Physics in 2025.

Data availability. The data that support the findings of this article are not publicly available upon publication because it is not technically feasible and/or the cost of preparing, depositing, and hosting the data would be prohibitive within the terms of this research project. The data are available from the authors upon reasonable request.

[1] T. Tajima and J. M. Dawson, Laser electron accelerator, Phys. Rev. Lett. **43**, 267 (1979).

[2] P. Chen, J. M. Dawson, R. W. Huff, and T. Katsouleas, Acceleration of electrons by the interaction of a bunched electron beam with a plasma, Phys. Rev. Lett. **54**, 693 (1985).

[3] A. Modena, Z. Najmudin, A. E. Dangor, C. E. Clayton, K. A. Marsh, C. Joshi, V. Malka, C. B. Darrow, C. Danson, D. Neely *et al.*, Electron acceleration from the breaking of relativistic plasma waves, Nature (London) **377**, 606 (1995).

[4] M. J. Hogan, C. D. Barnes, C. E. Clayton, F. J. Decker, S. Deng, P. Emma, C. Huang, R. H. Iverson, D. K. Johnson, C. Joshi *et al.*, Multi-GeV energy gain in a plasma-wakefield accelerator, Phys. Rev. Lett. **95**, 054802 (2005).

[5] A. J. Gonsalves, K. Nakamura, J. Daniels, C. Benedetti, C. Pieronek, T. C. H. de Raadt, S. Steinke, J. H. Bin, S. S. Bulanov, J. van Tilborg *et al.*, Petawatt laser guiding and electron beam acceleration to 8 GeV in a laser-heated capillary discharge waveguide, Phys. Rev. Lett. **122**, 084801 (2019).

[6] J. B. Rosenzweig, B. Breizman, T. Katsouleas, and J. J. Su, Acceleration and focusing of electrons in two-dimensional nonlinear plasma wake fields, Phys. Rev. A **44**, R6189 (1991).

[7] W. Lu, C. Huang, M. Zhou, W. B. Mori, and T. Katsouleas, Nonlinear theory for relativistic plasma wakefields in the blowout regime, Phys. Rev. Lett. **96**, 165002 (2006).

[8] I. Blumenfeld, C. E. Clayton, F.-J. Decker, M. J. Hogan, C. Huang, R. Ischebeck, R. Iverson, C. Joshi, T. Katsouleas, N. Kirby, W. Lu, K. A. Marsh, W. B. Mori, P. Muggli, E. Oz, R. H. Siemann, D. Walz, and M. Zhou, Energy doubling of 42 GeV electrons in a metre-scale plasma wakefield accelerator, Nature (London) **445**, 741 (2007).

[9] M. Litos *et al.*, High-efficiency acceleration of an electron beam in a plasma wakefield accelerator, Nature (London) **515**, 92 (2014).

[10] A. Caldwell, K. Lotov, A. Pukhov, and F. Simon, Proton-driven plasma-wakefield acceleration, Nat. Phys. **5**, 363 (2009).

[11] E. Adli, A. Ahuja, O. Apsimon, R. Apsimon, A.-M. Bachmann, D. Barrientos, F. Batsch, J. Bauche, V. K. Berglyd Olsen, M. Bernardini *et al.*, Acceleration of

electrons in the plasma wakefield of a proton bunch, Nature (London) **561**, 363 (2018).
[12] Y. P. Wu, J. F. Hua, Z. Zhou, J. Zhang, S. Liu, B. Peng, Y. Fang, Z. Nie, X. N. Ning, C.-H. Pai, Y. C. Du, W. Lu, C. J. Zhang, W. B. Mori, and C. Joshi, Phase space dynamics of a plasma wakefield dechirper for energy spread reduction, Phys. Rev. Lett. **122**, 204804 (2019).
[13] R. Pompili *et al.*, Energy spread minimization in a beam-driven plasma wakefield accelerator, Nat. Phys. **17**, 499 (2021).
[14] X. Wang, R. Ischebeck, P. Muggli, T. Katsouleas, C. Joshi, W. B. Mori, and M. J. Hogan, Positron injection and acceleration on the wake driven by an electron beam in a foil-and-gas plasma, Phys. Rev. Lett. **101**, 124801 (2008).
[15] N. Jain, T. M. Antonsen, and J. P. Palastro, Positron acceleration by plasma wakefields driven by a hollow electron beam, Phys. Rev. Lett. **115**, 195001 (2015).
[16] S. Diederichs, T. J. Mehrling, C. Benedetti, C. B. Schroeder, A. Knetsch, E. Esarey, and J. Osterhoff, Positron transport and acceleration in beam-driven plasma wakefield accelerators using plasma columns, Phys. Rev. Accel. Beams **22**, 081301 (2019).
[17] S. Diederichs, C. Benedetti, E. Esarey, J. Osterhoff, and C. B. Schroeder, High-quality positron acceleration in beam-driven plasma accelerators, Phys. Rev. Accel. Beams **23**, 121301 (2020).
[18] S. Zhou, J. Hua, W. An, W. B. Mori, C. Joshi, J. Gao, and W. Lu, High efficiency uniform wakefield acceleration of a positron beam using stable asymmetric mode in a hollow channel plasma, Phys. Rev. Lett. **127**, 174801 (2021).
[19] T. Silva, L. D. Amorim, M. C. Downer, M. J. Hogan, V. Yakimenko, R. Zgadzaj, and J. Vieira, Stable positron acceleration in thin, warm, hollow plasma channels, Phys. Rev. Lett. **127**, 104801 (2021).
[20] T. Silva and J. Vieira, Positron acceleration in plasma waves driven by Non-neutral fireball beams, Phys. Rev. Accel. Beams **26**, 091301 (2023).
[21] S. Diederichs, C. Benedetti, M. Thévenet, E. Esarey, J. Osterhoff, and C. B. Schroeder, Self-stabilizing positron acceleration in a plasma column, Phys. Rev. Accel. Beams **25**, 091304 (2022).
[22] B. E. Blue, C. E. Clayton, C. L. O'Connell, F.-J. Decker, M. J. Hogan, C. Huang, R. Iverson, C. Joshi, T. C. Katsouleas, W. Lu *et al.*, Plasma-wakefield acceleration of an intense positron beam, Phys. Rev. Lett. **90**, 214801 (2003).
[23] S. Corde, E. Adli, J. M. Allen, W. An, C. I. Clarke, C. E. Clayton, J. P. Delahaye, J. Frederico, S. Gessner, S. Z. Green *et al.*, Multi-gigaelectronvolt acceleration of positrons in a self-loaded plasma wakefield, Nature (London) **524**, 442 (2015).
[24] S. Lee, T. Katsouleas, R. G. Hemker, E. S. Dodd, and W. B. Mori, Plasma-wakefield acceleration of a positron beam, Phys. Rev. E **64**, 045501(R) (2001).
[25] H. Chen, S. C. Wilks, D. D. Meyerhofer, J. Bonlie, C. D. Chen, S. N. Chen, C. Courtois, L. Elberson, G. Gregori, W. Kruer *et al.*, Relativistic quasimonoenergetic positron jets from intense laser-solid interactions, Phys. Rev. Lett. **105**, 015003 (2010).
[26] H. Chen, S. C. Wilks, J. D. Bonlie, S. N. Chen, K. V. Cone, L. N. Elberson, G. Gregori, D. D. Meyerhofer, J. Myatt, D. F. Price *et al.*, Making relativistic positrons using ultraintense short pulse lasers, Phys. Plasmas **16**2009).
[27] H. Chen, F. Fiuza, A. Link, A. Hazi, M. Hill, D. Hoarty, S. James, S. Kerr, D. D. Meyerhofer, J. Myatt *et al.*, Scaling the yield of laser-driven electron-positron jets to laboratory astrophysical applications, Phys. Rev. Lett. **114**, 215001 (2015).
[28] C. P. Ridgers, C. S. Brady, R. Duclous, J. G. Kirk, K. Bennett, T. D. Arber, A. P. L. Robinson, and A. R. Bell, Dense electron-positron plasmas and ultraintense γ rays from laser-irradiated solids, Phys. Rev. Lett. **108**, 165006 (2012).
[29] G. J. Cao, C. A. Lindström, E. Adli, S. Corde, and S. Gessner, Positron acceleration in plasma wakefields, Phys. Rev. Accel. Beams **27**, 034801 (2024).
[30] Z. Y. Xu, C. F. Xiao, H. Y. Lu, R. H. Hu, J. Q. Yu, Z. Gong, Y. R. Shou, J. X. Liu, C. Z. Xie, S. Y. Chen *et al.*, New injection and acceleration scheme of positrons in the laser-plasma bubble regime, Phys. Rev. Accel. Beams **23**, 091301 (2020).
[31] T. Esirkepov, S. V. Bulanov, M. Yamagiwa, and T. Tajima, Electron, positron, and photon wakefield acceleration: Trapping, wake overtaking, and ponderomotive acceleration, Phys. Rev. Lett. **96**, 014803 (2006).
[32] E. Adli, Plasma wakefield linear colliders—opportunities and challenges, Phil. Trans. R. Soc. A **377**, 20180419 (2019).
[33] S. Steinke, J. Van Tilborg, C. Benedetti, C. G. R. Geddes, C. B. Schroeder, J. Daniels, K. K. Swanson, A. J. Gonsalves, K. Nakamura, N. H. Matlis *et al.*, Multistage coupling of independent laser-plasma accelerators, Nature (London) **530**, 190 (2016).
[34] Z. Jin, H. Nakamura, N. Pathak, Y. Sakai, A. Zhidkov, K. Sueda, R. Kodama, and T. Hosokai, Coupling effects in multistagelaser wake-field acceleration of electrons, Sci. Rep. **9**, 20045 (2019).
[35] Y. Wu, J. Hua, Z. Zhou, J. Zhang, S. Liu, B. Peng, Y. Fang, X. Ning, Z. Nie, F. Li *et al.*, High-throughput injection–Acceleration of electron bunches from a linear accelerator to a laser wakefield accelerator, Nat. Phys. **17**, 801 (2021).
[36] A. F. Pousa, R. Aßmann, A. Martinez de la Ossa *et al.*, VisualPIC: A new data visualizer and post-processor for particle-in-cell codes, in *Proceedings of the 8th Internationl Particle Accelerator Conference, 2017 (IPAC'17)* (2017), pp. 1696–1698.
[37] J. Vieira and J. T. Mendonça, Nonlinear laser driven donut wakefields for positron and electron acceleration, Phys. Rev. Lett. **112**, 215001 (2014).
[38] G.-B. Zhang, M. Chen, C. B. Schroeder, J. Luo, M. Zeng, F.-Y. Li, L.-L. Yu, S.-M. Weng, Y.-Y. Ma, T.-P. Yu *et al.*, Acceleration and evolution of a hollow electron beam in wakefields driven by a Laguerre-Gaussian laser pulse, Phys. Plasmas **23**, 033114 (2016).
[39] C. Baumann and A. Pukhov, Electron dynamics in twisted light modes of relativistic intensity, Phys Plasmas **25**, 083114 (2018).

[40] L. Reichwein, A. Pukhov, A. Golovanov, and I. Y. Kostyukov, Positron acceleration via laser-augmented blowouts in two-column plasma structures, Phys. Rev. E **105**, 055207 (2022).

[41] L. Fedeli, A. Huebl, F. Boillod-Cerneux, T. Clark, K. Gott, C. Hillairet, S. Jaure, A. Leblanc, R. Lehe, A. Myers, C. Piechurski, M. Sato, N. Zaim, W. Zhang, J.-L. Vay, and H. Vincenti, Pushing the frontier in the design of laser-based electron accelerators with groundbreaking mesh-refined particle-in-cell simulations on exascale-class supercomputers, in *SC22: International Conference for High Performance Computing, Networking, Storage and Analysis* (2022), pp. 1–12.

[42] E. Esarey, P. Sprangle, J. Krall, and A. Ting, Overview of plasma-based accelerator concepts, IEEE Trans. Plasma. Sci. **24**, 252 (1996).

[43] R. Keinigs and M. E. Jones, Two-dimensional dynamics of the plasma wakefield accelerator, Phys. Fluids **30**, 252 (1987).

[44] Z. Gong, Y. Shou, Y. Tang, R. Hu, J. Yu, W. Ma, C. Lin, and X. Yan, Proton sheet crossing in thin relativistic plasma irradiated by a femtosecond petawatt laser pulse, Phys. Rev. E **102**, 013207 (2020).

[45] Z. Gong, Y. Shou, Y. Tang, and X. Yan, Energetic spin-polarized proton beams from two-stage coherent acceleration in laser-driven plasma, Phys. Rev. E **102**, 053212 (2020).

[46] Z. Gong, M. J. Quin, S. Bohlen, C. H. Keitel, K. Põder, and M. Tamburini, Spin-polarized electron beam generation in the colliding-pulse injection scheme, Matter Radiat. Extremes **8**, 064005 (2023).

[47] I. Kostyukov, E. Nerush, A. Pukhov, and V. Seredov, Electron self-injection in multidimensional relativistic-plasma wake fields, Phys. Rev. Lett. **103**, 175003 (2009).

[48] S. Kalmykov, S. A. Yi, V. Khudik, and G. Shvets, Electron self-injection and trapping into an evolving plasma bubble, Phys. Rev. Lett. **103**, 135004 (2009).

[49] M. Tzoufras, W. Lu, F. S. Tsung, C. Huang, W. B. Mori, T. Katsouleas, J. Vieira, R. A. Fonseca, and L. O. Silva, Beam loading by electrons in nonlinear plasma wakes, Phys. Plasmas **16**, 056705 (2009).

[50] S. P. D. Mangles, A. G. R. Thomas, O. Lundh, F. Lindau, M. C. Kaluza, A. Persson, C.-G. Wahlström, K. Krushelnick, and Z. Najmudin, On the stability of laser wakefield electron accelerators in the monoenergetic regime, Phys. Plasmas **14**, 056702 (2007).

[51] X. L. Xu, F. Li, W. An, T. N. Dalichaouch, P. Yu, W. Lu, C. Joshi, and W. B. Mori, High quality electron bunch generation using a longitudinal density-tailored plasma-based accelerator in the three-dimensional blowout regime, Phys. Rev. Accel. Beams **20**, 111303 (2017).

[52] N. Jain, Evolution of Ultra-relativistic hollow electron beams during their propagation in plasmas, Phys. Plasmas **26**, 023107 (2019).

[53] See Supplemental Material at http://link.aps.org/supplemental/10.1103/n95z-ty9l for details of the evolution of hollow driver, the theoretical analysis of asymmetric drivers, and proton-driven acceleration.

[54] S. Diederichs, C. Benedetti, A. Huebl, R. Lehe, A. Myers, A. Sinn, J.-L. Vay, W. Zhang, and M. Thévenet, HiPACE++: A portable, 3D Quasi-static particle-in-cell code, Comput. Phys. Commun. **278**, 108421 (2022).

[55] L. Yi, B. Shen, L. Ji, K. Lotov, A. Sosedkin, X. Zhang, W. Wang, J. Xu, Y. Shi, L. Zhang *et al.*, Positron acceleration in a hollow plasma channel up to TeV regime, Sci. Rep. **4**, 4171 (2014).